processes

Article

Analytical Investigation on the Shear Propagation Mechanism of Multi-Cracks in Brittle Tight Rocks under Compressive and Shear Loading Conditions

Tianyu Luo, Qilin Wu *, Di Wu and Bin Li

Guangdong University of Petrochemical Technology, Maoming 525000, China; luotianyu88@foxmail.com (T.L.); 15092842683@139.com (D.W.)
* Correspondence: wuqilin1234@126.com

Abstract: There is abundant shale oil in the ocean and on land. Due to the tight lithology of the reservoir, volume fracturing technology is needed to improve the oil and gas productivity. It is very important to study the expansion law of multiple natural fractures in rock masses and its influencing factors in the process of volume fracturing for the formation of fracture networks. Based on the theory of online elastic fracture mechanics, the calculation method of the stress intensity factor at the end of any I–II composite fracture is established by using effective shear stress and considering the influence of T-stress. The calculation model of the stress intensity factor of any fracture on the main fracture wall or the horizontal section of the main fracture wall is established according to the concrete stress conditions in the process of hydraulic fracturing. Based on the principle of stress superposition, the combined interference stress calculation model of fracture ends is established for the case of multiple penetrating cracks in infinite-plane rock masses. Based on the theory of shear failure and plane strain, a model of the initiation direction and condition of natural cracks on the horizontal section of the main fracture wall and both sides of the main fracture in brittle rock is established when there are many coaxial natural cracks under the action of remote site stress and water pressure on the fracture surface. According to the simulation results, on the main fracture wall, when $\sigma_H > \sigma_v > \sigma_h$ or $\sigma_H > \sigma_h > \sigma_v$, when the crack angle (CA) is within a certain range and multiple natural cracks (MNC) exist, the required pressure for shear failure decreases. When the fracture angle exceeds a certain size, the required pressure increases. When there are MNC in the horizontal or perpendicular sections of the rock mass on both sides of the main fracture, the required net pressure for shear failure decreases within a certain CA range. When the CA exceeds a certain range, it increases or remains basically unchanged. On the whole, the presence of MNC reduces the net pressure for shear failure, which is conducive to the formation of fracture networks.

Keywords: brittle rock; volume fracturing; type I–II compound cracks; coaxial multi-cracks; shear failure

check for updates

Citation: Luo, T.; Wu, Q.; Wu, D.; Li, B. Analytical Investigation on the Shear Propagation Mechanism of Multi-Cracks in Brittle Tight Rocks under Compressive and Shear Loading Conditions. *Processes* **2023**, *11*, 1447. https://doi.org/10.3390/pr11051447

Academic Editors: Yinhui Zuo and Hui Han

Received: 23 March 2023
Revised: 13 April 2023
Accepted: 4 May 2023
Published: 10 May 2023

1. Introduction

Volume fracturing is an important tool for developing unconventional oil and gas fields. Unconventional oil and gas fields include shale gas and shale oil. Volume fracturing refers to the process of fracturing to form a longitudinal, three-dimensional fracture network in the formation, and to break up the reservoir so that the percolation distance of oil and gas is shortened and the resistance to percolation is reduced, thereby increasing oil and gas production. The development of MNC in brittle rocks (such as shale oil and shale gas) governs the formation of fracture networks [1,2]; however, the macroscopic failure laws of rock masses with MNC under different stresses have not been well explained so far. Therefore, it is of great significance to study the macrofailure law both in theory and in engineering practice.

Rock is a solid material with a very complex structure, which is a mixture of multiple mineral grains, cements, and pores. Rock defects, such as faults, joints, and fractures, have a significant impact on the mechanical properties of rocks. The essence of deformation and damage under various stresses during hydraulic fracturing is the process of the germination, expansion, interaction, and penetration of rock defects in the rock material, and so it is of great significance to study the mechanical properties of the tips of cracks (fractures).

The main types of fractures traditionally studied in fracture mechanics are opening-mode fractures (type I), sliding-mode fractures (type II), and tearing-mode fractures (type III). However, the forces in the actual structure are very complex, and so the stress field at the crack tip is usually composite, and compression–shear-complex-type cracks (CSCTCs) are the most common.

In recent years, several scientists around the world have achieved fruitful results in studying the expansion of destabilizing fractures and have developed appropriate failure criteria. There are two main types of fracture extension guidelines in common use currently: ① stress parameter methods: the maximum circumferential stress theory [3]; the Mises criterion; the Mohr–Coulomb criterion and Drucker–Prager criterion for the compression–shear failure criterion [4]; the Hoek–Brown criterion [5,6]; the maximum tensile strain [7]; the radial shear stress criterion [8]; the double shear stress criterion [8]; the minimum plastic radius criterion [9]; etc.; ② energy parameter methods: the strain energy density factor theory [10]; the maximum energy release rate theory [11]; the strain energy criterion for composite cracks [12]; the minimum J2 criterion [4,13,14]; and so on.

The central question to be answered is the extension angle at the crack tip and the mechanical conditions. Brittle failure includes two main forms, shear and tension [15–17]. In this paper, the shear failure theory is used to analyze the initiation law of natural cracks.

For the CSCTC problem, many scholars have conducted studies and obtained meaningful conclusions, but due to the complexity of the compression–shear failure problem, there are still many issues. At present, there are more studies on the rupture and extension law of hydraulic main fractures [18], but there are fewer studies on the opening and expansion law under which MNC form on the wall of the main fracture and on the horizontal section during the formation of the main fracture. However, this targeted research is critical to the formation of fracture networks.

Meanwhile, previous studies on compression–shear-complex-type failure problems have focused on the opening and expansion law of single fractures, but less under the condition of MNC. It is clear from the experiments that the load-carrying capacity of a single fractured body will be higher than that of an MNC body of the same type, and the stress intensity factor of the latter is increased [19,20]. During hydraulic fracturing, it is common for there to be MNC on the wall, and so it is necessary to study the corresponding crack opening and expansion law. In the same infinite plane, the relationship between MNC can be divided into parallel cracks and non-parallel cracks (intersecting cracks; non-intersecting coaxial cracks), where non-intersecting coaxial cracks will develop into intersecting ones. In summary, this paper focuses on the formation and propagation law and influencing factors of shear failure of multiple coaxial natural fractures on brittle rock walls around main fractures during hydraulic fracturing.

2. Calculation of Stress Intensity Factor of Multiple Fractures

2.1. Calculation of Stress Intensity Factor

This paper aims to reveal the opening rules of MNC on the main fracture wall under the action of fracturing fluid pressure in the process of hydraulic fracturing. The following assumptions are introduced: (1) the studied rock belongs to a brittle material and conforms to the linear elastic strain law, such as shale oil and shale gas; (2) the rock material is isotropic; (3) the natural cracks are ideal, of which the size is much smaller than that of the rock mass, while the rock mass size is infinite; (4) regardless of physical strength; (5) the fracture is of the penetrating type.

In the process of hydraulic fracturing, it is assumed that the vertical main fracture has been formed. On the wall of the main fracture, there are several coaxial penetration cracks, which belong to type I–II composite cracks. As shown in Figure 1, the circumferential pressure is uniformly distributed on the distal edge of the infinite rock mass, which is σ'_y and σ'_x. Taking the first fracture as the target fracture (TF), the influence of other fractures on the stress field for the end of the TF is studied. The Cartesian coordinate system x′oy′ (the x′ axis and y′ axis are parallel to the distal σ'_x and σ'_y, respectively) and the Cartesian coordinate system xoy (the x-axis is parallel to the fracture direction, and the y-axis is coplanar with the fracture central axis) are established. It is assumed that the angle between the direction of the TF and the action direction of σ'_y is β (called the crack angle), and that the angle between the j-th fracture and the TF is γ_j. The fluid pressure is the p_0 inside the fracture (y = 0, ∣x∣ < a, a is the fracture half-length).

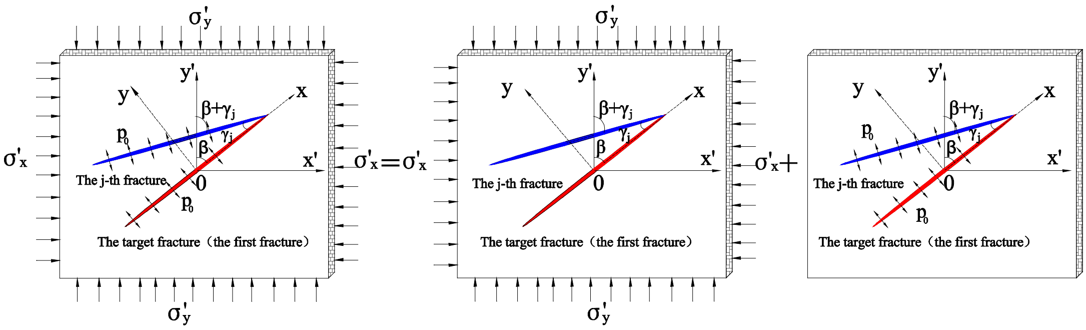

Figure 1. Hydraulic fracturing mechanical model and application of superposition principle of I–II composite fractures in compressed brittle rock.

Based on the above assumptions, the hydraulic fracturing mechanical model of I–II CSCTCs in brittle rock is shown in Figure 1a. The stress sign adopts the convention of elastic mechanics, with the tensile stress being positive and the compressive stress being negative. When the moment of shear stress to any point in the element body is clockwise, it is positive.

As shown in Figure 1, the fracture propagation problem (problem a) of an infinite rock mass under the action of uniform biaxial pressure on the edge and water pressure on the fracture surface can be transformed into the superposition of problem b and problem c.

For problem b, set in the coordinate system xoy, the stresses on the distal edge of an infinitely large rock mass are σ_x (corresponding to the x-axis), σ_y (corresponding to the y-axis), and τ_{xy}. For the j-th fracture, they are $\sigma_{x(j)}$, $\sigma_{y(j)}$, and $\tau_{xy(j)}$. Coordinate transformation between coordinate system x′oy′ and coordinate system xoy is carried out to obtain the stress in coordinate system xoy:

$$\left.\begin{array}{l}\sigma_{x(j)} = \sigma'_{\mathrm{y}} \cos^2(\gamma_j+\beta) + \sigma'_{\mathrm{x}} \sin^2(\gamma_j+\beta) \\ \sigma_{y(j)} = \sigma'_{\mathrm{y}} \sin^2(\gamma_j+\beta) + \sigma'_{\mathrm{x}} \cos^2(\gamma_j+\beta) \\ \tau_{xy(j)} = (\sigma'_{\mathrm{y}} - \sigma'_{\mathrm{x}}) \sin(\gamma_j+\beta) \cos(\gamma_j+\beta)\end{array}\right\} \tag{1}$$

According to the problem shown in Figure 1, the stress intensity factor at the end of the natural fracture can be obtained by applying the superposition principle according to the stress magnitude at the rock edge:

$$\left.\begin{array}{l}K_{\mathrm{I}a} = K_{\mathrm{I}b} + K_{\mathrm{I}c} \\ K_{\mathrm{II}a} = K_{\mathrm{II}b} + K_{\mathrm{II}c}\end{array}\right\} \tag{2}$$

For the j-th natural fracture in the rock mass, the effects of distal stress and intra-fracture pressure on the stress intensity factor at the fracture end are considered. In this paper, we only study the closure case, in which the intra-fracture pressure is not enough to make the fracture open. At this time, in the case of CSCTCs, the fracture is closed under compression, and there is friction on the upper and lower contact surfaces of the fracture in the process of fracture growth [21], which prevents the relative slipping and expansion.

When $\sigma_{y(j)}$ is the compressive stress (less than 0), the stress intensity factor at the end of type I caused by the distal compressive stress is negative, but it cannot be ignored as 0. First, the stress intensity factor caused by the intra-fracture pressure is positive, which tends to cause fracture expansion, which is reduced by the closure trend caused by the compressive stress. If the effect of $\sigma_{y(j)}$ compressive stress is not considered, then the effect of the expansion trend will be enlarged. In addition, the compressive stress creates a tendency to close the crack end, which does have an impact on the stress field at the crack end. Therefore, when the stress intensity factor is negative, it is a misunderstanding to regard this part of the stress intensity factor as 0.

The effective shear stress ($\boldsymbol{\tau}_{e(j)}$) should be used to calculate the type II end stress intensity factor (K_{II}). Since the direction of the shear force ($\left|\boldsymbol{\tau}_{xy(j)}\right|$) is always opposite to the shear resistance ($\tan\varphi\left|\sigma_{xy(j)}+p_0\right|$), which (positive and negative) may change, the calculation model of effective shear stress is as follows:

When the intra-fracture pressure (p_0) is smaller, $\left(\sigma_{y(j)}+p_0\right)<0$:

$$\boldsymbol{\tau}_{e(j)}=\begin{cases}0 & \left(\left|\boldsymbol{\tau}_{xy(j)}\right|<\tan\varphi\left|\sigma_{y(j)}+p_0\right|\right. \\ \boldsymbol{\tau}_{xy(j)}-\tan\varphi(\sigma_{y(j)}+p_0) & \left(\left|\boldsymbol{\tau}_{xy(j)}\right|>\tan\varphi\left|\sigma_{y(j)}+p_0\right|,(\sigma_{y(j)}+p_0)<0,\boldsymbol{\tau}_{xy(j)}>0\right. \\ \tan\varphi(\sigma_{y(j)}+p_0)-\boldsymbol{\tau}_{xy(j)} & \left(\left|\boldsymbol{\tau}_{xy(j)}\right|>\tan\varphi\left|\sigma_{y(j)}+p_0\right|,(\sigma_{y(j)}+p_0)<0,\boldsymbol{\tau}_{xy(j)}<0\right.\end{cases} \quad (3)$$

When the intra-fracture pressure (p_0) is larger, $\left(\sigma_{y(j)}+p_0\right)>0$:

$$\boldsymbol{\tau}_{e(j)}=\begin{cases}0 & \left(\left|\boldsymbol{\tau}_{xy(j)}\right|<\tan\varphi\left|\sigma_{y(j)}+p_0\right|\right. \\ \boldsymbol{\tau}_{xy(j)}-\tan\varphi(\sigma_{y(j)}+p_0) & \left(\left|\boldsymbol{\tau}_{xy(j)}\right|>\tan\varphi\left|\sigma_{y(j)}+p_0\right|,(\sigma_{y(j)}+p_0)>0,\boldsymbol{\tau}_{xy(j)}>0\right. \\ -\boldsymbol{\tau}_{xy(j)}-\tan\varphi(\sigma_{y(j)}+p_0) & \left(\left|\boldsymbol{\tau}_{xy(j)}\right|>\tan\varphi\left|\sigma_{y(j)}+p_0\right|,(\sigma_{y(j)}+p_0)>0,\boldsymbol{\tau}_{xy(j)}<0\right.\end{cases} \quad (4)$$

where φ is the angle of internal friction; for natural cracks, the size of cohesion is ignored. Then,

$$\left.\begin{array}{l}K_{I(j)}=K_{Ia(j)}=\left(\sigma_{y(j)}+p_0\right)\sqrt{\pi a} \\ K_{II(j)}=K_{IIa(j)}=\boldsymbol{\tau}_{e(j)}\sqrt{\pi a}\end{array}\right\} \quad (5)$$

2.2. Calculation of Stress Intensity Factor at the Fracture End of Any Fracture on the Main Fracture Wall

For the MNC on the wall of the main fracture (as shown in Figure 2), considering the actual stress status, in the rectangular coordinate system x′oy′, the rock mass edge is subjected to the forces $\sigma'_y=-\sigma_v$ in the vertical direction (σ_v is the vertical principal stress) and $\sigma'_x=-\sigma_H$ in the horizontal direction (σ_H is the maximum horizontal principal stress). For convenience, we let $\sigma_v=k\sigma_H$ (k > 0). On the fracture surface (y = 0, |x| < a), the pressure is p_0.

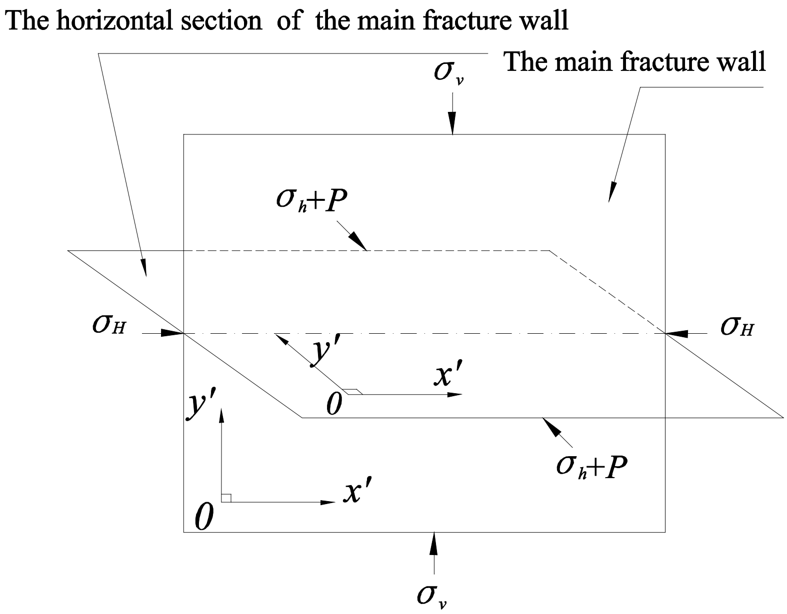

Figure 2. Schematic diagram of main fracture wall stress.

For the j-th fracture, according to (1), considering the actual stress status and the stress sign, the following results can be obtained:

$$\left.\begin{aligned} \sigma_{x(j)} &= -\sigma_{\rm v}\cos^2(\gamma_j+\beta) - \sigma_{\rm H}\sin^2(\gamma_j+\beta) \\ \sigma_{y(j)} &= -\sigma_{\rm v}\sin^2(\gamma_j+\beta) - \sigma_{\rm H}\cos^2(\gamma_j+\beta) \\ \boldsymbol{\tau}_{xy(j)} &= (\sigma_{\rm H}-\sigma_{\rm v})\sin(\gamma_j+\beta)\cos(\gamma_j+\beta) \end{aligned}\right\} \tag{6}$$

The expression of the stress intensity factor is obtained as follows:

$$\left.\begin{aligned} K_{{\rm I}(j)} &= [p_0 - (\sigma_{\rm v}\sin^2(\gamma_j+\beta) + \sigma_H\cos^2(\gamma_j+\beta))]\sqrt{\pi a} \\ K_{{\rm II}(j)} &= \boldsymbol{\tau}_{e(j)}\sqrt{\pi a} \end{aligned}\right\} \tag{7}$$

where $\boldsymbol{\tau}_{e(j)}$ (see Equations (3) and (4)). For the TF, it can be regarded as a special case, where γ_1 = 0 (j = 1).

2.3. Calculation of Stress Intensity Factor of Any Fracture on the Horizontal Section of the Main Fracture Wall

For the horizontal section on the main fracture wall (as shown in Figure 2), there are MNC on the surface, and the circumferential pressures on the distal edge are uniformly distributed, which are σ'_y and σ'_x. In this case, the pressure on the main fracture wall due to the expansion of the main fracture is $(\sigma_{\rm h}+P)$, where P is the net pressure in the fracture. That is, the part pressure exceeds the minimum principal stress ($\sigma_{\rm h}$). Then, after considering the stress sign, $\sigma'_y = -\sigma_{\rm h} - P$, $\sigma'_x = -\sigma_{\rm H}$. In natural fracture surfaces (y = 0, ∣x∣ < a), the pressure is p_0 (when the fracturing fluid pressure is not conductive to natural fracture, and the stress size is equal to the pore pressure). According to Equation (1), combined with the actual situation, the following equations can be obtained:

$$\left.\begin{aligned} \sigma_{x(j)} &= (-\sigma_{\rm h}-P)\cos^2(\gamma_j+\beta) - \sigma_{\rm H}\sin^2(\gamma_j+\beta) \\ \sigma_{y(j)} &= (-\sigma_{\rm h}-P)\sin^2((_j+\beta) - \sigma_{\rm H}\cos^2(\gamma_j+\beta) \\ \boldsymbol{\tau}_{xy(j)} &= (\sigma_{\rm H}-\sigma_{\rm h}-P)\sin(\gamma_j+\beta)\cos(\gamma_j+\beta) \end{aligned}\right\} \tag{8}$$

$$\left.\begin{aligned} K_{{\rm I}(j)} &= [p_0 - \sigma_{\rm h}\sin^2(\gamma_j+\beta) - P\sin^2(\gamma_j+\beta) - \sigma_H\cos^2(\gamma_j+\beta)]\sqrt{\pi a} \\ K_{{\rm II}(j)} &= \boldsymbol{\tau}_{e(j)}\sqrt{\pi a} \end{aligned}\right\} \tag{9}$$

For another type of section perpendicular to the main crack wall, considering the stress sign, $\sigma'_y = -\sigma_h - P$, $\sigma'_x = -\sigma_v$. The derivation of the stress intensity is similar to the above process.

3. Calculation of Multi-Fracture Stress Interference

There are multiple coaxial natural cracks with linear shapes in rock masses, and the stress state at the crack tip is calculated using elastic mechanics theory. For natural cracks with complex shapes, some scholars have also adopted the displacement discontinuity method (DDM) to model problems containing fractures [22].

As shown in Figure 3, the TF is taken as the research target fracture, which is located in the horizontal direction. It is assumed that the j-th fracture is coaxial with the TF, and the angle between the fractures is given as γ_j.

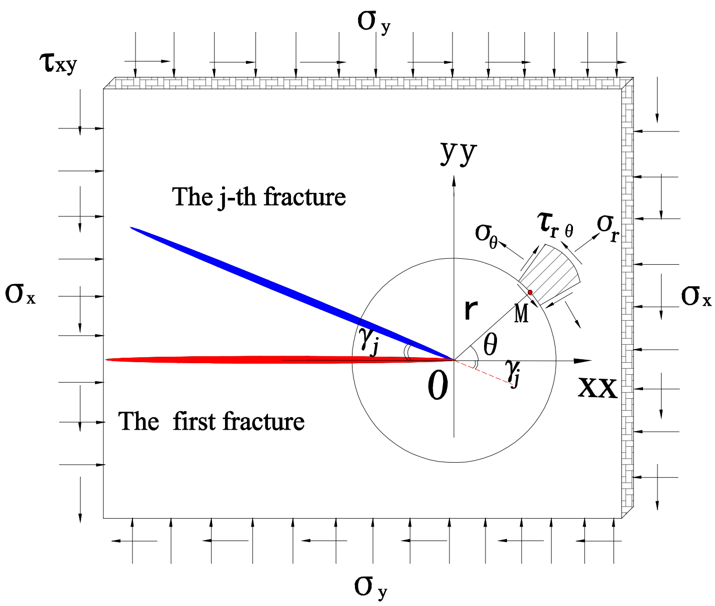

Figure 3. Schematic diagram of stress superposition calculation of multi-fracture ends.

The polar coordinates with the fracture end as the origin (called the fracture front coordinate system) is introduced. According to the traditional failure criterion, only the singular stress term in Williams expansion is used, and the non-singular stress term is often ignored. The recent research results show that the non-singular stress term T-stress of Williams expansion has an important influence on the fracture initiation angle, and the proposed theory is more consistent with the experimental results than the traditional theoretical calculation of the fracture initiation angle [17,23–25].

According to the linear elasticity theory, under the action of distal stress, in the polar coordinate system near the fracture tip of the TF, the polar coordinate expression of stress at the circumferential angle (θ) (corresponding to point M) in the unit circle with the radius (r) is as follows [16]:

$$\left.\begin{array}{l}
\sigma_{r(1)} = \frac{1}{2\sqrt{2\pi r}}\left[K_{I(1)}(3-\cos\theta)\cos\frac{\theta}{2} + K_{II(1)}(3\cos\theta - 1)\sin\frac{\theta}{2}\right] + T_{(1)}\cos^2\theta + N_{(1)}\sin^2\theta \\
\sigma_{\theta(1)} = \frac{1}{2\sqrt{2\pi r}}\cos\frac{\theta}{2}\left[K_{I(1)}(1+\cos\theta) - 3K_{II(1)}\sin\theta\right] + T_{(1)}\cos^2\theta + N_{(1)}\sin^2\theta \\
\boldsymbol{\tau}_{r\theta(1)} = \frac{1}{2\sqrt{2\pi r}}\cos\frac{\theta}{2}\left[K_{I(1)}\sin\theta + K_{II(1)}(3\cos\theta - 1)\right] - (T_{(1)} - N_{(1)})\cos\theta\sin\theta
\end{array}\right\} \quad (10)$$

where $\sigma_{r(1)}$ is the axial stress at point M on the unit circle circumference at the tip of the first fracture in the polar coordinate system; $\sigma_{\theta(1)}$ is the axial stress at point M; $\boldsymbol{\tau}_{r\theta(1)}$ is the shear stress at point M; $K_{I(1)}$ is the type II stress intensity factor of the TF (dimensionless); $K_{II(1)}$ is the type II stress intensity factor of the TF (dimensionless); r is the unit circle radius;

$T_{(1)}$ is the T-stress component parallel to the fracture surface of the TF (MPa); $N_{(1)}$ is the T-stress component perpendicular to the fracture surface of the TF (MPa).

For the TF, when the fracture is under compression stress, the T-stress is calculated as follows:

$$\left.\begin{array}{l} T_{(1)} = \sigma_{x(1)} \\ N_{(1)} = \sigma_{y(1)} \end{array}\right\} \tag{11}$$

For any j-th fracture, the singular term of the stress component at point M in polar coordinates is expressed by the following equation (in this case, the circumferential angle of point M in its polar coordinates is (γ_j + θ)):

$$\left.\begin{array}{rl} \sigma_{r(j)} = & \frac{1}{2\sqrt{2\pi r}}\left[K_{I(j)}(3-\cos(\theta+\gamma_j))\cos\frac{\theta+\gamma_j}{2} + K_{II(j)}(3\cos(\theta+\gamma_j)-1)\sin\frac{\theta+\gamma_j}{2}\right] \\ & +T_{(j)}\cos^2(\theta+\gamma_j) + N_{(j)}\sin^2(\theta+\gamma_j) \\ \sigma_{\theta(j)} = & \frac{1}{2\sqrt{2\pi r}}\cos\frac{\theta+\gamma_j}{2}\left[K_{I(j)}(1+\cos(\theta+\gamma_j)) - 3K_{II(j)}\sin(\theta+\gamma_j)\right] \\ & +T_{(j)}\sin^2(\theta+\gamma_j) + N_{(j)}\cos^2(\theta+\gamma_j) \\ \boldsymbol{\tau}_{r\theta(j)} = & \frac{1}{2\sqrt{2\pi r}}\cos\frac{\theta+\gamma_j}{2}\left[K_{I(j)}\sin(\theta+\gamma_j) + K_{II(j)}(3\cos(\theta+\gamma_j)-1)\right] \\ & -(T_{(j)} - N_{(j)})\sin(\theta+\gamma_j)\cos(\theta+\gamma_j) \end{array}\right\} \tag{12}$$

Among them,

$$\left.\begin{array}{l} T_{(j)} = \sigma_{x(j)} \\ N_{(j)} = \sigma_{y(j)} \end{array}\right\} \tag{13}$$

where $\sigma_{r(j)}$ is the axial stress at point M on the unit circle circumference at the tip of the j-th fracture in the polar coordinate system (MPa); $\sigma_{\theta(j)}$ is the radial stress at point M (MPa); $\boldsymbol{\tau}_{r\theta(j)}$ is the shear stress at point M (MPa); $K_{I(j)}$ is the type I stress intensity factor of the j-th fracture (dimensionless); $K_{II(j)}$ is the type II stress intensity factor of the j-th fracture (dimensionless); $T_{(j)}$ is the T-stress component parallel to the j-th fracture surface (MPa); $N_{(j)}$ is the T-stress component perpendicular to the j-th fracture surface (MPa).

Then, for the I–II composite fracture problem, the stress combination of n coaxial fractures at point M is as follows:

$$\sigma_r = \sum_{j=1}^{n}\sigma_{r(j)}\ \sigma_\theta = \sum_{j=1}^{n}\sigma_{\theta(j)}\ \boldsymbol{\tau}_r = \sum_{j=1}^{n}\sigma_{r\theta(j)} \tag{14}$$

where σ_r is the algebraic sum of axial stresses at the M point at the tip of n coaxial fractures in the polar coordinate system (MPa); σ_θ is the algebraic sum of radial stresses at M points at the tip of n coaxial fractures in the polar coordinate system (MPa); $\boldsymbol{\tau}_{r\theta}$ is the algebraic sum of shear stresses at the M point at the tip of n coaxial fractures in the polar coordinate system (MPa).

According to the stress at the end of each fracture, the stress at point M can be obtained when combined:

$$\left.\begin{array}{l} \sigma_r = \sum\limits_{j=1}^{n}\left\{\begin{array}{ll} \frac{1}{2\sqrt{2\pi r}} & \left[K_{I(j)}(3-\cos(\theta+\gamma_j))\cos\frac{\theta+\gamma_j}{2} + K_{II(j)}(3\cos(\theta+\gamma_j)-1)\sin\frac{\theta+\gamma_j}{2}\right] \\ & +\sigma_{x(j)}\cos^2(\theta+\gamma_j) + \sigma_{y(j)}\sin^2(\theta+\gamma_j) \end{array}\right\} \\ \sigma_\theta = \sum\limits_{j=1}^{n}\left\{\begin{array}{ll} \frac{1}{2\sqrt{2\pi r}} & \cos\frac{\theta+\gamma_j}{2}\left[K_{I(j)}(1+\cos(\theta+\gamma_j)) - 3K_{II(j)}\sin(\theta+\gamma_j)\right] \\ & +\sigma_{x(j)}\sin^2(\theta+\gamma_j) + \sigma_{y(j)}\cos^2(\theta+\gamma_j) \end{array}\right\} \\ \boldsymbol{\tau}_{r\theta} = \sum\limits_{j=1}^{n}\left\{\begin{array}{ll} \frac{1}{2\sqrt{2\pi r}} & \cos\frac{\theta+\gamma_j}{2}\left[K_{I(j)}\sin(\theta+\gamma_j) + K_{II(j)}(3\cos(\theta+\gamma_j)-1)\right] \\ & -(\sigma_{x(j)} - \sigma_{y(j)})\sin(\theta+\gamma_j)\cos(\theta+\gamma_j) \end{array}\right\} \end{array}\right\} \tag{15}$$

According to the above formula, the stress at any angle on the unit circle of the fracture tip can be obtained.

4. Multi-Fracture Shear Failure Model and Its Application

4.1. Shear Failure Model

4.1.1. Shear Failure Theory

In this paper, the shear failure theory is used to analyze fracture initiation. According to shear fracture theory: (1) the propagation direction of shear initiation is consistent with angle $\theta = \theta_0$, at which the absolute value of shear stress $|\tau_{r\theta}|$ reaches the maximum; (2) when the absolute value of shear stress reaches the shear strength (τ_c), fracture propagation begins. The description is as follows:

$$\left.\frac{d\boldsymbol{\tau}_{r\theta}}{d\theta}\right|_{r=r_0} = 0, \left.\frac{d^2|\boldsymbol{\tau}_{r\theta}|}{d\theta^2}\right|_{r=r_0} < 0 \tag{16}$$

$$|\boldsymbol{\tau}_{r\theta}|_{\max} = \boldsymbol{\tau}_c = |\sigma_{\theta_0}| \tan\varphi \tag{17}$$

When T-stress is considered, the term containing the critical distance (r_e) of the fracture tip cannot be eliminated when calculating the CA and circumferential stress. At present, there is no unified view on the determination of the r_e, which is often regarded as the characteristic attribute of materials. Most scholars use the following formula to estimate it [26]:

$$r_e = \frac{1}{2\pi}\left(\frac{K_{Ic}}{\sigma_t}\right)^2 \tag{18}$$

where K_{Ic} is the stress intensity factor; σ_t is the tensile strength.

4.1.2. The Angle and Conditions of Fracture Initiation and Expansion

When there is one fracture, according to Equation (15),

$$\begin{aligned}\sigma_{\theta(1)} = &\tfrac{1}{2\sqrt{2\pi r}} \cos\tfrac{\theta}{2}\left[K_{I(1)}(1+\cos\theta) - 3K_{II(1)}\sin\theta\right] \\ &+ \sigma_{x(1)}\sin^2\theta + \sigma_{y(1)}\cos^2\theta\end{aligned} \tag{19}$$

$$\begin{aligned}\boldsymbol{\tau}_{r\theta(1)} = &\tfrac{1}{2\sqrt{2\pi r}} \cos\tfrac{\theta}{2}\left[K_{I(1)}\sin\theta + K_{II(1)}(3\cos\theta - 1)\right] \\ &-(\sigma_{x(1)} - \sigma_{y(1)})\sin\theta\cos\theta\end{aligned} \tag{20}$$

According to shear failure theory Equation (16) and then (20), the following conditions are obtained for the initiation angle ($\theta = \theta_0$);

$$\begin{aligned}&\tfrac{d\boldsymbol{\tau}_{r\theta(1)}}{d\theta} = \tfrac{1}{2\sqrt{2\pi r_e}}\left[\begin{array}{l} K_{I(1)}\cos\theta_0\cos\frac{\theta_0}{2} - \frac{1}{2}K_{I(1)}\sin\theta_0\sin\frac{\theta_0}{2} \\ -3K_{II(1)}\sin\theta_0\cos\frac{\theta_0}{2} - \frac{1}{2}K_{II(1)}(3\cos\theta_0 - 1)\sin\frac{\theta_0}{2}\end{array}\right] \\ &-(\sigma_{x(1)} - \sigma_{y(1)})\cos 2\theta_0 = 0\end{aligned} \tag{21}$$

That is:

$$\begin{aligned}&\tfrac{1}{2\sqrt{2\pi r_e}}\left[\begin{array}{l} K_{I(1)}\cos\theta_0\cos\frac{\theta_0}{2} - \frac{1}{2}K_{I(1)}\sin\theta_0\sin\frac{\theta_0}{2} \\ -3K_{II(1)}\sin\theta_0\cos\frac{\theta_0}{2} - \frac{1}{2}K_{II(1)}(3\cos\theta_0 - 1)\sin\frac{\theta_0}{2}\end{array}\right] \\ &-(\sigma_{x(1)} - \sigma_{y(1)})\cos 2\theta_0 = 0\end{aligned} \tag{22}$$

According to shear failure theory Equation (17), the initiation conditions meet the following:

$$\begin{aligned} & abs\left\{\frac{1}{2\sqrt{2\pi r_e}}\cos\frac{\theta_0}{2}\left[K_{\mathrm{I}(1)}\sin\theta_0+K_{\mathrm{II}(1)}(3\cos\theta_0-1)\right]-(\sigma_{x(1)}-\sigma_{y(1)})\sin\theta_0\cos\theta_0\right\} \\ & = abs\left\{\frac{\tan\varphi}{2\sqrt{2\pi r_e}}\cos\frac{\theta_0}{2}\left[K_{\mathrm{I}(1)}(1+\cos\theta_0)-3K_{\mathrm{II}(1)}\sin\theta_0\right]+\sigma_{x(1)}\tan\varphi\sin^2\theta_0+\sigma_{y(1)}\tan\varphi\cos^2\theta_0\right\} \end{aligned} \tag{23}$$

When there are MNC, according to shear theory Equation (16) and stress superposition Equation (15), the shear failure initiation angle ($\theta = \theta_0$) meets the following conditions after stress superposition:

$$\frac{d\tau_{r\theta}}{d\theta}=\sum_{j=1}^{n}\left\{\begin{array}{l}\frac{1}{2\sqrt{2\pi r_e}}\left[\begin{array}{l}K_{\mathrm{I}(j)}\cos(\theta_0+\gamma_j)\cos(\frac{\theta_0+\gamma_j}{2})\\-\frac{1}{2}K_{\mathrm{I}(j)}\sin(\theta_0+\gamma_j)\sin(\frac{\theta_0+\gamma_j}{2})\\-3K_{\mathrm{II}(j)}\sin(\theta_0+\gamma_j)\cos(\frac{\theta_0+\gamma_j}{2})\\-\frac{1}{2}K_{\mathrm{II}(j)}(3\cos(\theta_0+\gamma_j)-1)\sin(\frac{\theta_0+\gamma_j}{2})\end{array}\right]\\-(\sigma_{x(j)}-\sigma_{y(j)})\cos 2(\theta_0+\gamma_j)\end{array}\right\}=0 \tag{24}$$

That is,

$$\sum_{j=1}^{n}\left\{\begin{array}{l}\frac{1}{2\sqrt{2\pi r_e}}\left[\begin{array}{l}K_{\mathrm{I}(j)}\cos(\theta_0+\gamma_j)\cos(\frac{\theta_0+\gamma_j}{2})\\-\frac{1}{2}K_{\mathrm{I}(j)}\sin(\theta_0+\gamma_j)\sin(\frac{\theta_0+\gamma_j}{2})\\-3K_{\mathrm{II}(j)}\sin(\theta_0+\gamma_j)\cos(\frac{\theta_0+\gamma_j}{2})\\-\frac{1}{2}K_{\mathrm{II}(j)}(3\cos(\theta_0+\gamma_j)-1)\sin(\frac{\theta_0+\gamma_j}{2})\end{array}\right]\\-(\sigma_{x(j)}-\sigma_{y(j)})\cos 2(\theta_0+\gamma_j)\end{array}\right\}=0 \tag{25}$$

According to shear initiation theory Equation (17), the fracture initiation conditions meet the following:

$$\begin{aligned} & abs\left\{\sum_{j=1}^{n}\left\{\begin{array}{l}\frac{1}{2\sqrt{2\pi r}}\cos\frac{\theta_0+\gamma_j}{2}\left[K_{I(j)}\sin(\theta_0+\gamma_j)+K_{II(j)}(3\cos(\theta_0+\gamma_j)-1)\right]\\-(\sigma_{x(j)}-\sigma_{y(j)})\sin(\theta_0+\gamma_j)con(\theta_0+\gamma_j)\end{array}\right\}\right\} \\ & = abs\left\{\sum_{j=1}^{n}\left\{\begin{array}{l}\frac{\tan\varphi}{2\sqrt{2\pi r}}\cos\frac{\theta_0+\gamma_j}{2}\left[k_{I(j)}(1+\cos(\theta_o+\gamma_j))-3K_{II(j)}\sin(\theta_0+\gamma_j)\right]\\+\tan\varphi\sigma_{x(j)}\sin^2(\theta_o+\gamma_j)+\tan\varphi\sigma_{x(j)}\cos^2(\theta_o+\gamma_j)\end{array}\right\}\right\} \end{aligned} \tag{26}$$

4.2. Discussion

4.2.1. Shear Failure When Natural Fractures Exist on the Main Fracture Wall

Due to the large computational workload, for the case of MNC, only the variation law of shear failure pressure when two fractures exist is simulated to illustrate the impact of multiple natural fractures.

The specific calculation model for this situation is shown in the Appendix A.1. Take σ_H = 63.5 MPa, σ_h = 50.39 MPa, a = 0.05 m, ψ = 20°, γ_1 = 0, γ_2 = 30°, K_{Ic} = 1 MPa·m$^{0.5}$, and σ_t = 5 MPa. Let k = σ_v/σ_H, and consider k = 0.5, k = 0.85, and k = 1.2. According to the above model, when one fracture and two fractures are simulated under different CAs (10° ≦ β ≦ 90°), the p_0 value of shear failure can be calculated. The simulation results are shown in Table 1 and Figure 4.

Table 1. The P_0 (MPa) values of shear failure when natural fractures exist on the main fracture wall.

β/°	10	20	30	40	50	60	70	80	90	
One fracture p_0/MPa	48	36	20	10	2	10	20	31	36	σ_v = 31.75 MPa σ_H = 63.5 MPa σ_h = 50.39 MPa k = 0.5
Two fractures p_0/MPa	25	18	12	3	0.3	9	24	33	38	
β/°	10	20	30	40	50	60	70	80	90	
One fracture p_0/MPa	85	83	82	79	76	72	70	68	66	σ_v = 53.975 MPa σ_H = 63.5 MPa σ_h = 50.39 MPa k = 0.85
Two fractures p_0/MPa	83	81	79	76	73	72	71	72	73	
β/°	10	20	30	40	50	60	70	80	90	
One fracture p_0/MPa	80	83	86	89	94	98	100	102	103	σ_v = 76.2 MPa σ_H = 63.5 MPa σ_h = 50.39 MPa k = 1.2
Two fractures p_0/MPa	86	89	92	95	98	100	101	102	103	

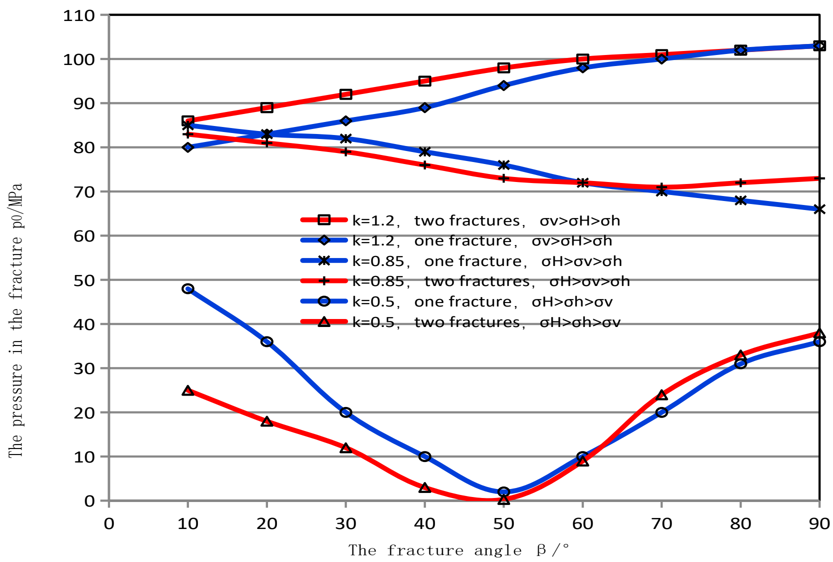

Figure 4. Simulation results of the p_0 values of shear failure when natural fractures exist on the main fracture wall.

According to the simulation results,

(1) When σ_H = 63.5 MPa, σ_h = 50.39 MPa, k = 1.2, σ_v = 76.2 MPa, and $\sigma_v > \sigma_H > \sigma_h$ (normal fault state), the pressure (p0) in the fracture is changed to produce shear failure. For one or two fractures, as the CA decreases, the required pressure to produce shear failure increases. Compared with one fracture, the required pressure in the presence of two fractures increases, and when the CA reaches a certain size, it remains unchanged;

(2) When σ_H = 63.5 MPa, σ_h = 50.39 MPa, k = 0.85, σ_v = 53.98 MPa, and $\sigma_H > \sigma_v > \sigma_h$, the vertical stress is the intermediate stress. For one or two fractures, with the CA increasing ($10° \leqq \beta \leqq 90°$), the required pressure decreases gradually. Compared with the case of smaller vertical stress (k = 0.5), the required pressure is higher due to the increase in vertical pressure. Compared with one fracture, when two fractures exist, the required pressure decreases, and when the CA reaches a certain value (about 60°), it increases. It can be seen that when the CA is within a certain range and MNC exist, the required pressure decreases, and when it exceeds a certain degree, it increases;

(3) When σ_H = 63.5 MPa, σ_h = 50.39 MPa, k = 0.5, σ_v = 31.75 MPa, and $\sigma_H > \sigma_h > \sigma_v$ (reverse fault state), for one or two fractures, as the CA increases, the required pressure is smaller, and after reaching a certain CA, it increases. Compared with one fracture,

the required pressure decreases, even lower than the pore pressure, and shear failure can occur. After reaching a certain CA, the required pressure increases. It can be seen that only in a certain angle range, when MNC exist, the required pressure decreases, and when exceeding a certain degree (about 50°), it increases.

4.2.2. Shear Failure When Natural Fractures Exist on the Horizontal Section

Let us start with two fractures. The specific calculation model for this situation is shown in the Appendix A.2.

The basic parameters are σ_h = 30 MPa; a = 0.05 m; ψ = 20°; γ_1 = 0; γ_2 = 30°; K_{Ic} = 1 MPa·m$^{0.5}$; σ_t = 5 MPa; p_0 = 30 MPa. According to the above model, when σ_h is fixed, the σ_H/σ_h is 2.52 (σ_H = 75.6 MPa) and 3.4 (σ_H = 100.8 MPa), respectively. When one fracture is simulated and two fractures are simulated, the net pressure (P) value for shear failure can be generated at the end under different CAs (10° ≦ β ≦ 90°). The simulation results are shown in Table 2 and Figure 5.

Table 2. Shear failure simulation results with MNC on horizontal sections.

β/°	10	20	30	40	50	60	70	80	90	
One fracture P/MPa	19.89	15.4	11.39	7.39	3.39	2.89	2.79	2.69	1.89	σ_h = 30 MPa σ_H = 75.6 MPa
Two fractures P/MPa	10.39	7.39	5.89	3.89	2.89	2.79	2.69	2.59	0.39	
β/°	10	20	30	40	50	60	70	80	90	
One fractureP/MPa	44.39	38.4	30.39	17.39	9.39	7.39	7.09	6.99	6.39	σ_h = 30 MPa σ_H = 100.8 MPa
Two fracturesP/MPa	30.39	22.39	16.89	13.39	14.29	17.09	16.99	16.39	12.39	

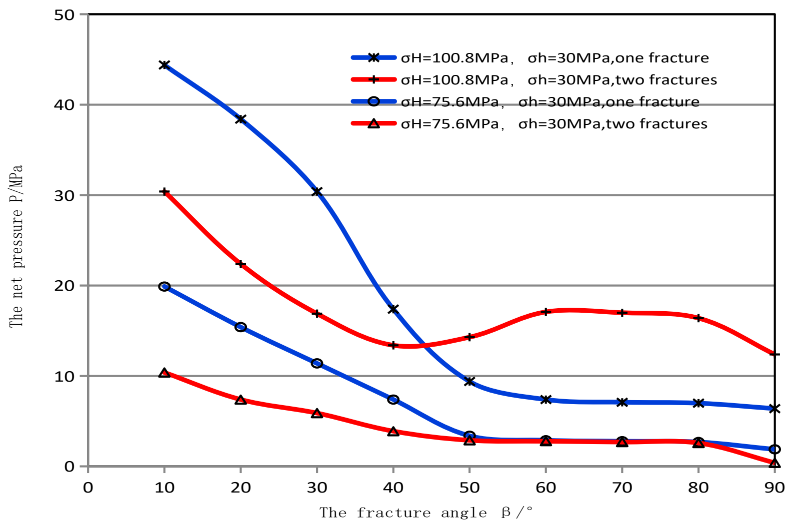

Figure 5. Simulation results of shear failure with MNC on horizontal sections.

According to the simulation results, for the shear failure situation with natural fractures on the horizontal section, the following applies:

(1) When σ_h = 30 MPa, σ_H/σ_h = 3.4, and σ_H = 100.8 MPa, we can change the net pressure (P) value on the distal end leading to the shear failure in the horizontal section. For one fracture, with the increase in the FA (the fracture direction tends to the direction of maximum principal stress), the required net failure pressure (NFP) decreases gradually, and it almost stays the same after reaching a certain angle (50°). When the CA reaches about 90°, the required NFP decreases slightly. When two fractures exist,

compared with one fracture, when $0 \leqq \beta \leqq 40°$, it decreases; when $40° \leqq \beta \leqq 90°$, it increases instead. It can be seen that when MNC exist, the required NFP decreases within a certain CA range. When the CA exceeds a certain size (about 40°), it increases;

(2) When σ_h = 30 MPa, σ_H/σ_h = 2.52, and σ_H = 75.6 MPa, compared with one fracture, when $0 \leqq \beta \leqq 50°$, the required NFP decreases gradually; when $50° \leqq \beta \leqq 80°$, the required NFPs are basically the same; when $80° \leqq \beta \leqq 90°$, it decreases accordingly. It can be seen that within a certain FA range, when MNC exist, the required NFP decreases. When the FA exceeds a certain size (about 50°), the required NFP is basically the same. Overall, the presence of MNC reduces the required NFP.

4.2.3. Shear Failure When Natural Fractures Exist on the Perpendicular Section Orthogonal to the Main Fracture Wall

The specific calculation model for this situation is shown in the Appendix A.3.

The basic parameters are σ_h = 30 MPa; a = 0.05 m; ψ = 20°; γ_1 = 0; γ_2 = 30°; K_{Ic} = 1 MPa·m$^{0.5}$; σ_t = 5 MPa; p_0 = 30 MPa. When σ_h is fixed, σ_v = 75.6 MPa and σ_v = 100.8 MPa. When one fracture or two fractures are simulated, the net pressure (P) value for shear failure can be generated at the end under different CAs ($10° \leqq \beta \leqq 90°$). The simulation results are shown in Table 3 and Figure 6.

Table 3. Shear failure simulation results with MNC on perpendicular sections orthogonal to the main fracture wall.

β/°	10	20	30	40	50	60	70	80	90	
One fracture P/MPa	19.89	15.4	11.39	7.39	3.39	2.89	2.79	2.69	1.89	σ_h = 30 MPa σ_v = 75.6 MPa
Two fractures P/MPa	10.39	7.39	5.89	3.89	2.89	2.79	2.69	2.59	0.39	
β/°	10	20	30	40	50	60	70	80	90	
One fracture P/MPa	44.39	38.4	30.39	17.39	9.39	7.39	7.09	6.99	6.39	σ_h = 30 MPa σ_v = 100.8 MPa
Two fractures P/MPa	30.39	22.39	16.89	13.39	14.29	17.09	16.99	16.39	12.39	

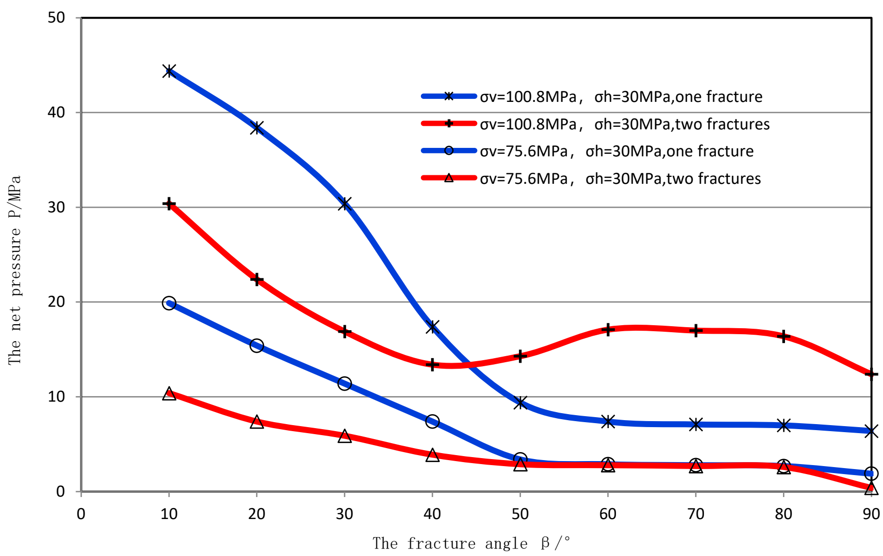

Figure 6. Simulation results of shear failure with MNC on perpendicular sections orthogonal to the main fracture wall.

According to the simulation results, for the shear failure situation with natural fractures on the horizontal section orthogonal to the main fracture wall, the following applies:

(1) When σ_h = 30 MPa, σ_v = 100.8 MPa, for one fracture, with the increase in the FA (the fracture direction tends to the direction of maximum principal stress), the required net failure pressure (NFP) decreases gradually, and it almost stays the same after reaching a certain angle (50°). When the CA reaches about 90°, the required NFP decreases slightly. When two fractures exist, compared with one fracture, when $0 \leqq \beta \leqq 40°$, it decreases; when $40° \leqq \beta \leqq 90°$, it increases instead. It can be seen that when MNC exist, the required NFP decreases within a certain CA range. When the CA exceeds a certain size (about 40°), it increases;

(2) When σ_h = 30 MPa, σ_v = 75.6 MPa, compared with one fracture, when $0 \leqq \beta \leqq 50°$, the required NFP decreases gradually; when $50° \leqq \beta \leqq 80°$, the required NFPs are basically the same; when $80° \leqq \beta \leqq 90°$, it decreases accordingly. It can be seen that within a certain FA range, when MNC exist, the required NFP decreases. When the FA exceeds a certain size (about 50°), the required NFP is basically the same. Overall, the presence of MNC reduces the required NFP.

4.2.4. Confirmation of the Research Results

Through the research, compared to one fracture, the shear failure pressure corresponding to two fractures significantly decreased, the degree of reduction of which is related to the boundary load and the fracture angle. The work of many scholars has verified the rationality of the research results above.

Through experimental research and finite element analysis, it has been concluded that under the same stress-level conditions, multi-crack specimens are more prone to failure than single-crack specimens due to the mutual influence between fractures [20].

Different crack inclination angles have different effects on the macroscopic strength of multi-crack rocks. The experiment found that as the angle between the core direction and the bedding plane increases, the failure mode of the rock sample gradually changes [27].

When two elliptical fractures merge with each other, the stress intensity factor increases sharply at the contact point compared to other locations [28].

When there are multi-cracks, the maximum percentage of decrease in the failure peak is 18.8%; as the fracture angle increases, the maximum percentage of decrease in the failure peak is 61.9%[29].

From the experimental and numerical investigations, it was found that the failure strength and Young's modulus decrease by increasing the joint number [30].

5. Conclusions

In the process of hydraulic fracturing, it is very common that multiple natural cracks in brittle rock expand simultaneously and interact with each other. In the past, the study of CSCTCs focused on the failure law of a single fracture, and the fracture propagation law under the condition of the simultaneous existence of MNC was rarely studied. In this paper, the position relationship of MNC is considered, and the principle of stress superposition is adopted to establish the criterion of the shear initiation and propagation of the target fracture under the conditions of compression and shear, and under the influence of adjacent fractures. Combined with the need for fracture network formation in the process of hydraulic fracturing, this paper mainly studies the fracture initiation direction and initiation condition model of MNC on the wall of the main fracture and the horizontal section and perpendicular sections orthogonal to the main fracture wall.

According to the simulation, when natural fractures exist on the main fracture wall, the following applies:

- When $\sigma_v > \sigma_H > \sigma_h$ (normal fault state), compared with one fracture, the pressure required for shear failure in the presence of two fractures increases, and the difficulty of shear failure increases. When the CA reaches a certain size, the pressure required for shear failure tends to be similar;

- When $\sigma_H > \sigma_v > \sigma_h$, compared with one fracture, when the CA is within a certain range, the pressure required for shear failure decreases, and when the CA exceeds a certain degree, it increases;
- When $\sigma_H > \sigma_h > \sigma_v$ (reverse fault state), compared with one fracture, only within a certain FA range, when MNC exist, the required pressure decreases, and when it exceeds a certain degree (about 50°, under simulated conditions), the required pressure increases.

To the horizontal or perpendicular sections of the rock mass on both sides of the main fracture, the following applies:

- For one fracture, with the increase in the FA (the fracture direction tends to the direction of maximum principal stress), the required net failure pressure (NFP) decreases gradually, and it almost stays the same after reaching a certain angle (50–80°).When the CA reaches about 80°–90°, the required NFP decreases slightly;
- When two fractures exist, compared with one fracture, when $0 \leqq \beta \leqq 40°$, the required net pressure decreases; when $50° \leqq \beta \leqq 90°$, it increases ($\sigma_h$ = 30 MPa, σ_v = 100.8 MPa, or σ_H = 100.8 MPa) or remains basically unchanged (σ_h = 30 MPa, σ_v = 75.6 MPa, or σ_H = 75.6 MPa). It can be seen that when MNC exist, the required NFP decreases within a certain CA range. It increases or remains basically unchanged when the CA exceeds a certain size.

On the whole, the presence of MNC reduces the required net pressure during shear failure, which is conducive to the formation of fracture networks. The above model and application simulation reveal the internal mechanism of forming complex fracture networks in main fracture wall rock masses in the process of the hydraulic fracturing of brittle rock.

Author Contributions: Conceptualization, Q.W. and T.L.; methodology, T.L.; software, T.L. and D.W.; validation, T.L. and Q.W.; formal analysis, T.L. and D.W.; investigation, B.L.; resources, B.L.; data curation, Q.W.; writing—original draft preparation, T.L.; writing—review and editing, D.W.; visualization, Q.W.; supervision, Q.W.; project administration, T.L.; funding acquisition, Q.W. All authors have read and agreed to the published version of the manuscript.

Funding: This research was funded by the Project of Introducing Top-notch Talents Urgently Needed in Guangdong Province's Sail Plan for Talents Development (grant number:917003) and the Characteristic Innovation Project of Guangdong Provincial Department of Education (grant number: 2019KTSCX103).

Data Availability Statement: Our research data is authentic and reliable, but the data is unavailable due to privacy or ethical restrictions. If any scholars are interested in the calculation process, they can contact the authors to obtain.

Acknowledgments: Thanks to all the comrades of petroleum engineering Department of petroleum engineering College.

Conflicts of Interest: The authors declare no conflict of interest.

Appendix A

Appendix A.1. Formula Derivation

According to (25), combined with Equations (6) and (7), and substituted with the stress intensity factor, the conditions satisfying the fracture initiation angle can be obtained as follows:

$$\mathrm{A}_{(1)} + \mathrm{A}_{(2)} = 0 \tag{A1}$$

Among them,

$$\mathrm{A}_{(1)} = \frac{\sqrt{\pi a}}{2\sqrt{2\pi r_e}} \begin{bmatrix} [p_0 - (\sigma_v \sin^2\beta + \sigma_H \cos^2\beta)]\left(\cos\theta_0 \cos\frac{\theta_0}{2} - \frac{1}{2}\sin\theta_0 \sin\frac{\theta_0}{2}\right) \\ +\boldsymbol{\tau}_{e(1)}\left[-3\sin\theta_0\cos\frac{\theta_0}{2} - \frac{1}{2}(3\cos\theta_0 - 1)\sin\frac{\theta_0}{2}\right] \end{bmatrix} \tag{A2}$$
$$-(\sigma_v \sin^2\beta + \sigma_H \cos^2\beta - \sigma_v \cos^2\beta - \sigma_H \sin^2\beta)\cos 2\theta_0$$

$$\mathrm{A}_{(2)} = \frac{\sqrt{\pi a}}{2\sqrt{2\pi r_e}}\left[\begin{array}{l} [p_0 - (\sigma_v \sin^2(\beta+\gamma_2) + \sigma_H \cos^2(\beta+\gamma_2))]\cdot \\ \left[\cos(\theta_0+\gamma_2)\cos\left(\frac{\theta_0+\gamma_2}{2}\right) - \frac{1}{2}\sin(\theta_0+\gamma_2)\sin\left(\frac{\theta_0+\gamma_2}{2}\right)\right] \\ +\boldsymbol{\tau}_{e(2)}\left[-3\sin(\theta_0+\gamma_2)\cos\left(\frac{\theta_0+\gamma_2}{2}\right) - \frac{1}{2}(3\cos(\theta_0+\gamma_2)-1)\sin\left(\frac{\theta_0+\gamma_2}{2}\right)\right] \end{array}\right] \\ -\left[\sigma_v \sin^2(\beta+\gamma_2) + \sigma_H \cos^2(\beta+\gamma_2) - \sigma_v \cos^2(\beta+\gamma_2) - \sigma_H \sin^2(\beta+\gamma_2)\right]\cos 2(\theta_0+\gamma_2) \tag{A3}$$

According to shear initiation theory Equation (26), the fracture initiation conditions meet the following:

$$\mathrm{abs}(\mathrm{CZZ}_{(1)} + \mathrm{CZZ}_{(2)}) = abs(\mathrm{CZY}_{(1)} + \mathrm{CZY}_{(2)}) \tag{A4}$$

Among them,

$$\mathrm{CZZ}_{(1)} = \frac{\sqrt{\pi a}}{2\sqrt{2\pi r_e}}\cos\frac{\theta_0}{2}\left\{[p_0 - \sigma_v \sin^2\beta - \sigma_H \cos^2\beta]\sin\theta_0 + \boldsymbol{\tau}_{e(1)}(3\cos\theta_0 - 1)\right\} \\ -(\sigma_v \sin^2\beta + \sigma_H \cos^2\beta - \sigma_v \cos^2\beta - \sigma_H \sin^2\beta)\sin\theta_0\cos\theta_0 \tag{A5}$$

$$\mathrm{CZZ}_{(2)} = \frac{\sqrt{\pi a}}{2\sqrt{2\pi r_e}}\cos\left(\frac{\theta_0+\gamma_2}{2}\right)\left\{\begin{array}{l} [p_0 - \sigma_v \sin^2(\beta+\gamma_2) - \sigma_H \cos^2(\beta+\gamma_2)]\sin(\theta_0+\gamma_2) \\ +\boldsymbol{\tau}_{e(1)}(3\cos(\theta_0+\gamma_2) - 1) \end{array}\right\} \\ -\left[\sigma_v \sin^2(\beta+\gamma_2) + \sigma_H \cos^2(\beta+\gamma_2) - \sigma_v \cos^2(\beta+\gamma_2) - \sigma_H \sin^2(\beta+\gamma_2)\right]\sin(\theta_0+\gamma_2)\cos(\theta_0+\gamma_2) \tag{A6}$$

$$\mathrm{CZY}_{(1)} = \frac{\tan\varphi\sqrt{\pi a}}{2\sqrt{2\pi r_e}}\cos\frac{\theta_0}{2}\left[[p_0 - \sigma_v \sin^2\beta - \sigma_H \cos^2\beta](1+\cos\theta_0) - 3\boldsymbol{\tau}_{e(1)}\sin\theta_0\right] \\ -(\sigma_v \cos^2\beta + \sigma_H \sin^2\beta)\tan\varphi\sin^2\theta_0 - (\sigma_v \sin^2\beta + \sigma_H \cos^2\beta)\tan\varphi\cos^2\theta_0 \tag{A7}$$

$$\mathrm{CZY}_{(2)} = \frac{\tan\varphi\sqrt{\pi a}}{2\sqrt{2\pi r_e}}\cos\left(\frac{\theta_0+\gamma_2}{2}\right)\left[\begin{array}{l} [p_0 - (\sigma_v \sin^2(\beta+\gamma_2) + \sigma_H \cos^2(\beta+\gamma_2))](1+\cos(\theta_0+\gamma_2)) \\ -3\boldsymbol{\tau}_{e(1)}\sin(\theta_0+\gamma_2) \end{array}\right] \\ -\left[\sigma_v \cos^2(\beta+\gamma_2) + \sigma_H \sin^2(\beta+\gamma_2)\right]\tan\varphi\sin^2(\theta_0+\gamma_2) \\ -\left[\sigma_v \sin^2(\beta+\gamma_2) + \sigma_H \cos^2(\beta+\gamma_2)\right]\tan\varphi\cos^2(\theta_0+\gamma_2) \tag{A8}$$

When only the TF exists, the initiation angle meets the following conditions:

$$\mathrm{A}_{(1)} = 0 \tag{A9}$$

The fracture initiation conditions meet the following:

$$\mathrm{abs}(\mathrm{CZZ}_{(1)}) = abs(\mathrm{CZY}_{(1)}) \tag{A10}$$

Appendix A.2. Formula Derivation

Let us start with two fractures. According to Equation (25), after substituting the stress intensity factor and stress into Equations (8) and (9), the conditions satisfying the fracture initiation angle can be obtained as follows:

$$\mathrm{B}_{(1)} + \mathrm{B}_{(2)} = 0 \tag{A11}$$

Among them,

$$\mathrm{B}_{(1)} = \frac{\sqrt{\pi a}}{2\sqrt{2\pi r_e}}\left[\begin{array}{l} \left[p_0 - (\sigma_h + P)\sin^2\beta - \sigma_H \cos^2\beta\right]\cdot \\ \left[\cos\theta_0\cos\frac{\theta_0}{2} - \frac{1}{2}\sin\theta_0\sin\frac{\theta_0}{2}\right] \\ -3\boldsymbol{\tau}_{e(1)}\sin\theta_0\cos\frac{\theta_0}{2} - \frac{1}{2}\boldsymbol{\tau}_{e(1)}(3\cos\theta_0 - 1)\sin\frac{\theta_0}{2} \end{array}\right] \\ -\left[-(\sigma_h + P)\cos^2\beta - \sigma_H \sin^2\beta + (\sigma_h + P)\sin^2\beta + \sigma_H \cos^2\beta\right]\cos 2\theta_0 \tag{A12}$$

$$B_{(2)} = \frac{\sqrt{\pi a}}{2\sqrt{2\pi r_e}} \left[\begin{array}{l} \left[p_0 - (\sigma_h + P)\sin^2(\gamma_2+\beta) - \sigma_H \cos^2(\gamma_2+\beta)\right] \cdot \\ \left[\cos(\theta_0+\gamma_2)\cos\left(\frac{\theta_0+\gamma_2}{2}\right) - \frac{1}{2}\sin(\theta_0+\gamma_2)\sin(\frac{\theta_0+\gamma_2}{2})\right] \\ -3\boldsymbol{\tau}_{e(2)}\sin(\theta_0+\gamma_2)\cos\left(\frac{\theta_0+\gamma_2}{2}\right) \\ -\frac{1}{2}\boldsymbol{\tau}_{e(2)}(3\cos(\theta_0+\gamma_2)-1)\sin\left(\frac{\theta_0+\gamma_2}{2}\right) \end{array} \right]$$
$$- \left[\begin{array}{l} -(\sigma_h + P)\cos^2(\gamma_2+\beta) - \sigma_H \sin^2(\gamma_2+\beta) \\ +(\sigma_h + P)\sin^2(\gamma_2+\beta) + \sigma_H \cos^2(\gamma_2+\beta) \end{array} \right] \cos 2(\theta_0+\gamma_2) \quad \text{(A13)}$$

According to shear initiation theory Equation (26), the fracture initiation condition meets the following:

$$\text{abs}(\text{SPZ}_{(1)} + \text{SPZ}_{(2)}) = abs(\text{SPY}_{(1)} + \text{SPY}_{(2)}) \quad \text{(A14)}$$

Among them,

$$\text{SPZ}_{(1)} = \frac{\sqrt{\pi a}}{2\sqrt{2\pi r_e}} \cos\frac{\theta_0}{2} \left\{ \begin{array}{l} \left[p_0 - (\sigma_h + P)\sin^2\beta - \sigma_H\cos^2\beta\right]\sin\theta_0 \\ +\boldsymbol{\tau}_{e(2)}(3\cos\theta_0 - 1) \end{array} \right\}$$
$$- \left[\begin{array}{l} -(\sigma_h + P)\cos^2\beta - \sigma_H\sin^2\beta \\ +(\sigma_h + P)\sin^2\beta + \sigma_H\cos^2\beta \end{array} \right] \sin\theta_0\cos\theta_0 \quad \text{(A15)}$$

$$\text{SPZ}_{(2)} = \frac{\sqrt{\pi a}}{2\sqrt{2\pi r_e}} \cos\frac{\theta_0+\gamma_2}{2} \left\{ \begin{array}{l} \left[p_0 - (\sigma_h + P)\sin^2(\gamma_2+\beta) - \sigma_H\cos^2(\gamma_2+\beta)\right]\sin(\theta_0+\gamma_2) \\ +\boldsymbol{\tau}_{e(2)}(3\cos(\theta_0+\gamma_2) - 1) \end{array} \right\}$$
$$- \left[\begin{array}{l} -(\sigma_h + P)\cos^2(\gamma_2+\beta) - \sigma_H\sin^2(\gamma_2+\beta) \\ +(\sigma_h + P)\sin^2(\gamma_2+\beta) + \sigma_H\cos^2(\gamma_2+\beta) \end{array} \right] \sin(\theta_0+\gamma_2)\cos(\theta_0+\gamma_2) \quad \text{(A16)}$$

$$\text{SPY}_{(1)} = \frac{\tan var\phi}{2\sqrt{2\pi r_e}} \cos\frac{\theta_0}{2} \left\{ \begin{array}{l} \left[p_0 - (\sigma_h + P)\sin^2\beta - \sigma_H\cos^2\beta\right] \cdot \\ (1 + \cos\theta_0 - 3\boldsymbol{\tau}_{e(2)}\sin\theta_0 \end{array} \right\}$$
$$+ \tan\varphi\left[-(\sigma_h + P)\cos^2\beta - \sigma_H\sin^2\beta\right]\sin^2\theta_0$$
$$+ \tan\varphi\left[-(\sigma_h + P)\sin^2\beta - \sigma_H\cos^2\beta\right]\cos^2\theta_0 \quad \text{(A17)}$$

$$\text{SPY}_{(2)} = \frac{\tan\varphi}{2\sqrt{2\pi r_e}} \cos\frac{\theta_0+\gamma_2}{2} \left\{ \begin{array}{l} \left[p_0 - (\sigma_h + P)\sin^2(\gamma_2+\beta) - \sigma_H\cos^2(\gamma_2+\beta)\right] \cdot \\ (1 + \cos)\theta_0 + \gamma_2)) - 3\boldsymbol{\tau}_{e(2)}\sin(\theta_0+\gamma_2) \end{array} \right\}$$
$$+ \tan\varphi\left[-(\sigma_h + P)\cos^2(\gamma_2+\beta) - \sigma_H\sin^2(\gamma_2+\beta)\right]\sin^2(\theta_0+\gamma_2)$$
$$+ \tan\varphi\left[-(\sigma_h + P)\sin^2(\gamma_2+\beta) - \sigma_H\cos^2(\gamma_2+\beta)\right]\cos^2(\theta_0+\gamma_2) \quad \text{(A18)}$$

When there is only one fracture, the shear initiation angle meets the following conditions:

$$\text{B}_{(1)} = 0 \quad \text{(A19)}$$

In this case, the shear failure initiation condition meets the following:

$$\text{abs}(\text{SPZ}_{(1)}) = abs(\text{SPY}_{(1)}) \quad \text{(A20)}$$

Appendix A.3. Formula Derivation

Let us start with two fractures. According to Equation (25), after substituting the stress intensity factor and stress into Equations (8) and (9), the conditions satisfying the fracture initiation angle can be obtained as follows:

$$\text{C}_{(1)} + \text{C}_{(2)} = 0 \quad \text{(A21)}$$

Among them,

$$C_{(1)} = \frac{\sqrt{\pi a}}{2\sqrt{2\pi r_e}} \begin{bmatrix} \left[p_0 - (\sigma_h + P)\sin^2\beta - \sigma_v \cos^2\beta\right] \cdot \\ \left[\cos\theta_0 \cos\frac{\theta_0}{2} - \frac{1}{2}\sin\theta_0 \sin\frac{\theta_0}{2}\right] \\ -3\boldsymbol{\tau}_{e(1)} \sin\theta_0 \cos\frac{\theta_0}{2} - \frac{1}{2}\boldsymbol{\tau}_{e(1)}(3\cos\theta_0 - 1)\sin\frac{\theta_0}{2} \end{bmatrix} \\ -\left[-(\sigma_h + P)\cos^2\beta - \sigma_v \sin^2\beta + (\sigma_h + P)\sin^2\beta + \sigma_v \cos^2\beta\right]\cos 2\theta_0 \tag{A22}$$

$$C_{(2)} = \frac{\sqrt{\pi a}}{2\sqrt{2\pi r_e}} \begin{bmatrix} \left[p_0 - (\sigma_h + P)\sin^2(\gamma_2 + \beta) - \sigma_v \cos^2(\gamma_2 + \beta)\right] \cdot \\ \left[\cos(\theta_0 + \gamma_2)\cos\left(\frac{\theta_0 + \gamma_2}{2}\right) - \frac{1}{2}\sin(\theta_0 + \gamma_2)\sin\left(\frac{\theta_0 + \gamma_2}{2}\right)\right] \\ -3\boldsymbol{\tau}_{e(2)} \sin(\theta_0 + \gamma_2)\cos\left(\frac{\theta_0 + \gamma_2}{2}\right) \\ -\frac{1}{2}\boldsymbol{\tau}_{e(2)}(3\cos(\theta_0 + \gamma_2) - 1)\sin\left(\frac{\theta_0 + \gamma_2}{2}\right) \end{bmatrix} \\ -\begin{bmatrix} -(\sigma_h + P)\cos^2(\gamma_2 + \beta) - \sigma_v \sin^2(\gamma_2 + \beta) \\ +(\sigma_h + P)\sin^2(\gamma_2 + \beta) + \sigma_v \cos^2(\gamma_2 + \beta) \end{bmatrix} \cos 2(\theta_0 + \gamma_2) \tag{A23}$$

According to shear initiation theory Equation (26), the fracture initiation condition meets the following:

$$\mathrm{abs}(\mathrm{CZQZ}_{(1)} + \mathrm{CZQZ}_{(2)}) = abs(\mathrm{CZQY}_{(1)} + \mathrm{CZQY}_{(2)}) \tag{A24}$$

Among them,

$$\mathrm{CZQZ}_{(l)} = \frac{\sqrt{\pi a}}{2\sqrt{2\pi r_e}} \cos\frac{\theta_0}{2} \begin{Bmatrix} \left[p_0 - (\sigma_h + P)\sin^2\beta - \sigma_v \cos^2\beta\right]\sin\theta_0 \\ +\boldsymbol{\tau}_{e(2)}(3\cos\theta_0 - 1) \end{Bmatrix} \\ -\begin{bmatrix} -(\sigma_h + P)\cos^2\beta - \sigma_v \sin^2\beta \\ +(\sigma_h + P)\sin^2\beta + \sigma_v \cos^2\beta \end{bmatrix} \sin\theta_0 \cos\theta_0 \tag{A25}$$

$$\mathrm{CZQZ}_{(2)} = \frac{\sqrt{\pi a}}{2\sqrt{2\pi r_e}} \cos\frac{\theta_0 + \gamma_2}{2} \begin{Bmatrix} \left[p_0 - (\sigma_h + P)\sin^2(\gamma_2 + \beta) - \sigma_v \cos^2(\gamma_2 + \beta)\right]\sin(\theta_0 + \gamma_2) \\ +\boldsymbol{\tau}_{e(2)}(3\cos(\theta_0 + \gamma_2) - 1) \end{Bmatrix} \\ -\begin{bmatrix} -(\sigma_h + P)\cos^2(\gamma_2 + \beta) - \sigma_v \sin^2(\gamma_2 + \beta) \\ +(\sigma_h + P)\sin^2(\gamma_2 + \beta) + \sigma_v \cos^2(\gamma_2 + \beta) \end{bmatrix} \sin(\theta_0 + \gamma_2)\cos(\theta_0 + \gamma_2) \tag{A26}$$

$$\mathrm{CZQY}_{(1)} = \frac{\tan\varphi}{2\sqrt{2\pi r_e}} \cos\frac{\theta_0}{2} \begin{Bmatrix} \left[p_0 - (\sigma_h + P)\sin^2\beta - \sigma_v \cos^2\beta\right] \cdot \\ (1 + \cos\theta_0 - 3\boldsymbol{\tau}_{e(2)} \sin\theta_0 \end{Bmatrix} \\ + \tan\varphi\left[-(\sigma_h + P)\cos^2\beta - \sigma_v \sin^2\beta\right]\sin^2\theta_0 \\ + \tan\varphi\left[-(\sigma_h + P)\sin^2\beta - \sigma_v \cos^2\beta\right]\cos^2\theta_0 \tag{A27}$$

$$\mathrm{CZQY}_{(2)} = \frac{\tan\varphi}{2\sqrt{2\pi r_e}} \cos\frac{\theta_0 + \gamma_2}{2} \begin{Bmatrix} \left[p_0 - (\sigma_h + P)\sin^2(\gamma_2 + \beta) - \sigma_v \cos^2(\gamma_2 + \beta)\right] \cdot \\ (1 + \cos)\theta_0 + \gamma_2)) - 3\boldsymbol{\tau}_{e(2)} \sin(\theta_0 + \gamma_2) \end{Bmatrix} \\ + \tan\varphi\left[-(\sigma_h + P)\cos^2(\gamma_2 + \beta) - \sigma_v \sin^2(\gamma_2 + \beta)\right]\sin^2(\theta_0 + \gamma_2) \\ + \tan\varphi\left[-(\sigma_h + P)\sin^2(\gamma_2 + \beta) - \sigma_v \cos^2(\gamma_2 + \beta)\right]\cos^2(\theta_0 + \gamma_2) \tag{A28}$$

When there is only one fracture, the shear initiation angle meets the following conditions:

$$C_{(1)} = 0 \tag{A29}$$

In this case, the shear failure initiation condition meets the following:

$$\mathrm{abs}(\mathrm{CZQZ}_{(1)}) = abs(\mathrm{CZQY}_{(1)}) \tag{A30}$$

References

1. Dou, L.B.; Yang, H.J.; Xiao, Y.J. Probability study of formation brittleness and new quantitative evaluation of fracability for shale reservoirs. *Prog. Geophys.* **2021**, *36*, 576–584. [CrossRef]
2. He, R.; Yang, Z.Z.; Li, X.G. A comprehensive approach for fracability evaluation in naturally fractured sandstone reservoirs based on analytical hierarchy process method. *Energy Sci. Eng.* **2019**, *7*, 529–545. [CrossRef]
3. Erdogan, F.; Sih, G.C. On the crack extension in plates under plane loading and transverse shear. *J. Flu. Eng.* **1963**, *85*, 519–527. [CrossRef]
4. Zhou, J.W.; Xu, W.Y.; Shi, C. Investigation on compression-shear fracture criterion of rock based on failure criteria. *Chin. J. Roc. Mec. Eng.* **2007**, *26*, 1194–1201.
5. Zhu, H.H.; Zhang, Q.; Zhang, L.Y. Review of research progresses and applications of Hoek-Brown strength criterion. *Chin. J. Roc. Mech. Eng.* **2013**, *32*, 1945–1963.
6. Zhu, Y.; Zhou, H.; Zhang, C.Q.; Lu, T. Brittle inequality of Hoek-Brown criterion and its applicability limit to GSI. *Chin. J. Roc. Mech. Eng.* **2018**, *38*, 3412–3419. [CrossRef]
7. Feng, Y.J.; Kang, H.P. The initiation of I-IImixed mode crack subjected to hydraulic pressure in brittle rock under compression. *J. China Coal. Soc.* **2013**, *38*, 226–232. [CrossRef]
8. Li, B.; Huang, R.Q.; Wu, L.Z. Compression-shear fracture criteria for mixed mode I-II of open crack of rock-like brittle materials. *Chin. J. Geo. Eng.* **2017**, *39*, 662–668.
9. Gao, W.; Cui, S.; Xiao, T.; Chen, X.; Zhou, C.; Hu, C.J. Crack initiation of rock based on the minimum plastic zone radius criterion. *J. China. Coal. Soc.* **2022**, *46*, 3193–3202. [CrossRef]
10. Nuismer, R.J. An energy release rate criterion for mixed mode fracture. *Int. J. Frac. Mech.* **1975**, *11*, 245–250. [CrossRef]
11. Zhao, Z.S. A strain energy criterion for mixed mode crack propagation. *Acta Mech. Solida Sin.* **1987**, *26*, 533–539.
12. Lin, B.S. The mixed mode brittle fracture criteria in sliding mode fracture. *Appl. Mat. Mec.* **1985**, *6*, 977–983.
13. Zhao, Y.H.; Xu, S.N. The minimum criterion for I-II mixed mode brittle fracture. *Eng. Mech.* **2002**, *19*, 94–98.
14. Sih, G.C. Energy-density concept in fracture mechanics. *Eng. Frac. Eng.* **1973**, *5*, 1037–1040. [CrossRef]
15. Paterson, M.S.; Wong, T. *Experimental Rock Deformation-The Brittle Field, 2nd ed*; Springer Science and Business Media: Berlin, Germany, 2005; p. 248.
16. Tang, S.; Huang, R.; Tang, C. Effect of T-stress on crack growth path in rock and fracture strength. *Rock Soil Mech.* **2016**, *37*, 1521–1529. [CrossRef]
17. Zhu, J.D.; Li, S.H.; Wu, L.Z. Hydraulic Fracturing Properties of Rock under Compression Considering T-stress. *Chin. J. Undergr. Spa. Eng.* **2019**, *15*, 1765–1771.
18. Ren, L.; Jiang, H.; Zhao, J.Z. A model for calculating breakdown pressure in deep perforated wells with considering wellbore deformation. *Pet. Geol. Oilfield Dev. Daqing* **2022**, *41*, 64–73. [CrossRef]
19. Li, L.Y.; Liu, D.; Shi, X.Q. Biaxial com-pression experiments and orthotropic constitutive re-lationship for regular cracks in replicated rock mass. *Chin. J. Nonferrous Met.* **2002**, *12*, 165–170.
20. Che, F.X.; Li, L.Y.; Liu, D.A. Fracture experments and finite element analysis for multi-cracks body of rock-like material. *Chin. J. Roc. Mech. Eng.* **2000**, *3*, 295–298.
21. Lü, T.; Zhao, M.J.; Wang, Y. Research on fracture criterion of compressed rock. *J. Undergr. Space Eng.* **2010**, *6*, 969–974.
22. Abdollahipour, A.; Marji, M.F. A thermo-hydromechanical displacement discontinuity method to model fractures in high-pressure, high-temperature environments. *Renew. Energy* **2020**, *153*, 1488–1503. [CrossRef]
23. Li, Y.J.; Ni, T.; Zuo, J.P.; Liu, D.J.; Song, Y.H. Analysis of crack initiation mechanism and influencing factors of the hard roof in directional hydraulic fracturing. *Chin. J. Roc. Mec. Eng.* **2022**, 2015–2029. [CrossRef]
24. Tang, S.B.; Zhang, H. The characteristics of crack initiation at the crack tip in rock material. *China J. Roc. Mec. Eng.* **2017**, *36*, 552–561. [CrossRef]
25. Jin, S.Y.; Liu, H. Study on the Influence of T Stress Component on the Tensile Initiation Angle of Compression-shear Closed Crack. *Pearl River* **2020**, *41*, 68–74. [CrossRef]
26. Aliha, M.R.M.; Ayatollahi, M.R. Two-parameter fracture analysis of SCB rock specimen under mixed mode loading. *Eng. Fract. Mech.* **2013**, *103*, 115–123. [CrossRef]
27. Liang, L.X.; Zhuang, D.L.; Liu, X.J.; Xiong, J. Study on Mechanical Properties and Failure Modes of Longmaxi Shale. *Chin. J. Undergr. Space Eng.* **2017**, *13*, 108–115.
28. Pang, C.; Liu, D.J.; Tian, G.; Guo, W.; Liu, D.B. Experimental and Simulation Study on Fatigue Multi Crack Fusion of 2195-T8 Al Li Alloy. *J. Beijing Univ. Aeronaut. Astronaut.* **2022**, 1–13. [CrossRef]
29. Zhao, N.; Li, W.Q.; Feng, J.Y.; Wang, Y.R.; Li, L. Numerical simulation and mechanism study on the influence of multi-crack on crack lap law. *Drill. Prod. Technol.* **2020**, *45*, 160–164. [CrossRef]
30. Haeri, H.; Sarfarazi, V.; Ebneabbasi, P.; Shahbazian, A.; Marji, M.F.; Mohamadi, A.R. XFEM and experimental simulation of failure mechanism of non-persistent joints in mortar under compression. *Constr. Build. Mater.* **2020**, *236*, 117500. [CrossRef]